Performance Analysis of ESPRIT-Type Algorithms for Co-Array Structures

Jens Steinwandt [1], *Florian Roemer* [2], *and Martin Haardt* [1]

[1] Communications Research Laboratory, Ilmenau University of Technology, P.O. Box 100565, 98684 Ilmenau, Germany
[2] Digital Broadcasting Laboratory, Ilmenau University of Technology, P.O. Box 100565, 98684 Ilmenau, Germany
Emails: {jens.steinwandt, florian.roemer, martin.haardt}@tu-ilmenau.de, Web: www.tu-ilmenau.de/crl

***Abstract*—In the recent field of co-array signal processing, sparse linear arrays are processed to form a virtual uniform linear array (ULA), termed co-array, that allows to resolve more sources than physical sensors. The extra degrees of freedom (DOFs) are leveraged by the assumption that the signals are uncorrelated, which requires a large sample size. In this paper, we first review the Standard ESPRIT and Unitary ESPRIT algorithms for co-array processing. Secondly, we propose a performance analysis for both methods, which is asymptotic in the effective signal-to-noise ratio (SNR), i.e., the results become exact for either high SNRs or a large sample size. Based on the derived analytical expressions, we study the effects of a small sample size such as the residual sample signal correlation and the sample noise contribution on the estimation accuracy of the proposed algorithms. Simulation results verify the derived analytical expressions.**

***Index Terms*—Performance analysis, ESPRIT, co-array, parameter estimation.**

I. Introduction

Extracting the directions of arrival (DOAs) of impinging signals plays a central role in sensor array signal processing [1]. This task is required in many applications such as radar, sonar, and wireless communications. Among the subspace-based parameter estimation algorithms, ESPRIT-type algorithms [2], [3] are often preferred due to their low complexity and their high-resolution capabilities.

It is well known that assuming an M-element uniform linear array (ULA), the conventional subspace-based DOA estimation algorithms such as MUSIC [1] and ESPRIT can resolve at most $M-1$ uncorrelated signals. To circumvent this limitation, an emerging interest has been on addressing the underdetermined DOA estimation problem, i.e., resolving more sources than the number of sensors. In particular, several sparse (non-uniform) linear array geometries such as minimum redundancy arrays (MRAs) [4], nested arrays [5], and co-prime arrays [6] have been proposed. These array structures allow for the construction of a larger virtual ULA, also termed co-array, that can resolve up to $\mathcal{O}(M^2)$ sensors by exploiting the signals' uncorrelated-ness to gain the additional degrees of freedom (DOF). The virtual co-array model represents a single snapshot model such that spatial smoothing preprocessing [8] is required before applying the conventional parameter estimation methods. For instance, spatial smoothing combined with the MUSIC algorithm for the co-array model has been proposed in [5]. However, ESPRIT-type algorithms for co-arrays [7] that are closed-form and less complex should be preferred.

As a drawback, co-array processing heavily relies on the assumption that the received signals, the noise samples, and the signals and the noise are statistically uncorrelated. However, only for the infinite sample case, the sample signal covariance matrix and the sample noise covariance matrix become diagonal and the sample signal-noise-cross-correlation matrix vanishes. Therefore, co-array-based DOA estimation algorithms only perform well in a large sample scenario. Yet, in practice, only a small sample size may be available, which leads to a performance degradation due to the residual sample signal correlation in the signal covariance matrix, the non-diagonal sample noise covariance matrix and the non-zero sample signal-noise correlation. The impact of these effects on the estimation accuracy of co-array-based DOA algorithms has so far not been analyzed.

Despite the growing research interest in co-array processing, the analytical performance of co-array-based DOA estimation algorithms still remains to be investigated. The performance of MUSIC and ESPRIT for the physical array model has been thoroughly studied in [9], [10], [11]. Note that the performance framework in [11] is more general than the one in [10] as the resulting first-order error expression is deterministic in the small noise contribution and thus does not require any assumptions on the noise statistics, e.g., Gaussianity. Moreover, it is asymptotic in the effective signal-to-noise ration (SNR), i.e., the results become accurate for either high SNRs or a large sample size. Hence, [11] is even valid for the small sample case if the SNR is sufficiently high. More recently, the performance of ESPRIT-type algorithms with spatial smoothing for the physical array model based on [11] has been derived in [12]. For the virtual co-array model, the analytical performance for co-array-based MUSIC was recently derived in [13].

In this paper, we first review the Standard ESPRIT and Unitary ESPRIT algorithms designed for co-array processing. Secondly, we present a first-order performance analysis for the mean square error (MSE) both methods adopting [11], which is asymptotic in the effective SNR and thus also valid for a small sample size. Based on these analytical expressions, we study the effects of a finite number of samples, resulting in a residual sample signal correlation and sample noise correlation, on the estimation accuracy of the proposed co-array-based Standard ESPRIT and Unitary ESPRIT algorithms. Simulation results verify the derived analytical expressions.

II. Data Model for Co-Arrays

Consider an M-element linear sparse antenna array whose sensors are located at the positions $\boldsymbol{k} = [k_1, \ldots, k_M] \cdot \delta$, where each sensor location $k_n,\ n = 1, \ldots, M$ is an integer multiple of the half-wavelength interelement spacing $\delta = \lambda/2$. Assume that the array receives d uncorrelated narrowband signals from the far field with the spatial frequencies $\mu_i = \frac{2\pi}{\lambda}\delta\sin(\theta_i),\ i = 1, \ldots, d$. The array steering vector corresponding to the i-th signal is given by

$$\boldsymbol{a}(\mu_i) = \begin{bmatrix} \mathrm{e}^{\mathrm{j}k_1\mu_i} & \mathrm{e}^{\mathrm{j}k_2\mu_i} & \ldots & \mathrm{e}^{\mathrm{j}k_M\mu_i} \end{bmatrix}^{\mathrm{T}} \in \mathbb{C}^{M\times 1}. \quad (1)$$

This work was partially supported by the DFG project EXPRESS (HA 2239/6-1) and the Carl-Zeiss Foundation under the scholarship project EM-BiCoS.

978-1-5386-1251-4/17/$31.00 ©2017 IEEE

The array response vectors can be expressed by the linear model

$$\boldsymbol{x}(t) = \boldsymbol{A}\boldsymbol{s}(t) + \boldsymbol{n}(t) \in \mathbb{C}^{M\times 1}, \quad t = 1, \ldots, N, \tag{2}$$

where $\boldsymbol{A} = [\boldsymbol{a}(\mu_1), \ldots, \boldsymbol{a}(\mu_d)] \in \mathbb{C}^{M\times d}$ is the array steering matrix, which contains the array steering vectors $\boldsymbol{a}(\mu_i)$ for the d spatial frequencies. The vector $\boldsymbol{s}(t) \in \mathbb{C}^{d\times 1}$ represents the source symbols, $\boldsymbol{n}(t) \in \mathbb{C}^{M\times 1}$ consists of the additive sensor noise samples, and N denotes the number of snapshots.

The spatial covariance matrix $\boldsymbol{R} \in \mathbb{C}^{M\times M}$ of (2) is given by

$$\boldsymbol{R} = \mathbb{E}\left\{\boldsymbol{x}(t)\boldsymbol{x}^{\mathrm{H}}(t)\right\} = \boldsymbol{A}\boldsymbol{R}_{\mathrm{ss}}\boldsymbol{A}^{\mathrm{H}} + \boldsymbol{A}\boldsymbol{R}_{\mathrm{sn}} + \boldsymbol{R}_{\mathrm{ns}}\boldsymbol{A}^{\mathrm{H}} + \boldsymbol{R}_{\mathrm{nn}}, \tag{3}$$

where $\boldsymbol{R}_{\mathrm{ss}} = \mathbb{E}\left\{\boldsymbol{s}(t)\boldsymbol{s}^{\mathrm{H}}(t)\right\} \in \mathbb{C}^{d\times d}$ is the signal covariance matrix, $\boldsymbol{R}_{\mathrm{sn}} = \mathbb{E}\left\{\boldsymbol{s}(t)\boldsymbol{n}^{\mathrm{H}}(t)\right\} \in \mathbb{C}^{d\times M}$ and $\boldsymbol{R}_{\mathrm{ns}} = \boldsymbol{R}_{\mathrm{sn}}^{\mathrm{H}}$ are the signal-noise cross-correlation matrices, and $\boldsymbol{R}_{\mathrm{nn}} = \mathbb{E}\left\{\boldsymbol{n}(t)\boldsymbol{n}^{\mathrm{H}}(t)\right\} \in \mathbb{C}^{M\times M}$ is the noise covariance matrix.

A. Infinite Sample Case

Assuming ergodicity of the signals and the noise, we make the following assumptions in the infinite sample scenario, i.e., $N \to \infty$:

- **A.1** The source signals are uncorrelated and circularly symmetric complex Gaussian distributed, i.e, $\boldsymbol{R}_{\mathrm{ss}} = \mathrm{diag}\{P_1, \ldots, P_d\} \in \mathbb{R}^{d\times d}$, where P_i is the power of the i-th signal.
- **A.2** The noise samples are white circularly symmetric complex Gaussian distributed with variance σ_{n}^2 and uncorrelated from the signals, i.e., $\boldsymbol{R}_{\mathrm{nn}} = \sigma_{\mathrm{n}}^2\boldsymbol{I}_M$ and $\boldsymbol{R}_{\mathrm{sn}} = \boldsymbol{R}_{\mathrm{ns}} = \boldsymbol{0}$.

Under these assumptions, the spatial covariance matrix $\boldsymbol{R}$ reduces to

$$\boldsymbol{R} = \boldsymbol{A}\boldsymbol{R}_{\mathrm{ss}}\boldsymbol{A}^{\mathrm{H}} + \sigma_{\mathrm{n}}^2\boldsymbol{I}_M. \tag{4}$$

Applying the vectorization operator to (4), we obtain the model

$$\boldsymbol{r} = \mathrm{vec}\{\boldsymbol{R}\} = \boldsymbol{A}_{\mathrm{c}}\boldsymbol{p} + \sigma_{\mathrm{n}}^2\boldsymbol{e} \in \mathbb{C}^{M^2\times 1}, \tag{5}$$

where $\boldsymbol{A}_{\mathrm{c}} = \boldsymbol{A}^* \diamond \boldsymbol{A} \in \mathbb{C}^{M^2\times d}$ with $\diamond$ denoting the Khatri-Rao product (column-wise Kronecker product). Moreover, $\boldsymbol{p} = [P_1, \ldots, P_d]^{\mathrm{T}} \in \mathbb{C}^{d\times 1}$ contains the signal powers and $\boldsymbol{e} = \mathrm{vec}\{\boldsymbol{I}_M\} \in \mathbb{R}^{M^2\times 1}$.

It was observed in [5] that (5) can be interpreted as a deterministic array response vector (single snapshot) of the virtual array described by $\boldsymbol{A}_{\mathrm{c}}$ that receives the source vector $\boldsymbol{p}$ under the sensor noise $\sigma_{\mathrm{n}}^2\boldsymbol{e}$. The matrix $\boldsymbol{A}_{\mathrm{c}}$ corresponds to the array steering matrix of the virtual array whose sensor positions are given by the difference set $\mathbb{D} = \{(k_m - k_n)\delta\},\ m, n = 1, \ldots, M$. Note that $\mathbb{D}$ contains several repeated virtual elements associated with the same sensor location. By selecting the consecutive virtual sensor positions and averaging over the repeated sensor elements of $\boldsymbol{A}_{\mathrm{c}}$ to reduce the sensor noise via the selection matrix $\boldsymbol{\Gamma}$ according to [13], a steering matrix $\boldsymbol{A}_{\mathrm{v}}$ corresponding to a virtual ULA can be constructed, i.e., $\boldsymbol{A}_{\mathrm{v}} = \boldsymbol{\Gamma}\boldsymbol{A}_{\mathrm{c}}$. Thus, we obtain the model

$$\boldsymbol{z} = \boldsymbol{\Gamma}\boldsymbol{r} = \boldsymbol{A}_{\mathrm{v}}\boldsymbol{p} + \sigma_{\mathrm{n}}^2\boldsymbol{\Gamma}\boldsymbol{e} \in \mathbb{C}^{M_{\mathrm{v}}\times 1}, \tag{6}$$

If the physical array is properly designed, the number of sensors M_{v} of the virtual ULA, which determines the degrees of freedom (DOF), can be larger than the number of sensors M of the physical array. The case $M_{\mathrm{v}} > M$ will be assumed throughout this work. Hence, by performing parameter estimation on the virtual array instead of the physical array, more sources than sensors can be resolved.

B. Finite Sample Case

In practice, the true covariance matrix $\boldsymbol{R}$ is not available and usually estimated by its sample covariance matrix. To this end, the N consecutive snapshots of the measurement data are expressed in matrix form as $\boldsymbol{X} = \boldsymbol{A}\boldsymbol{S} + \boldsymbol{N} \in \mathbb{C}^{M\times N}$, where $\boldsymbol{S} \in \mathbb{C}^{d\times N}$ and $\boldsymbol{N} \in \mathbb{C}^{M\times N}$ contain the symbol vectors $\boldsymbol{s}(t)$ and the noise vectors $\boldsymbol{n}(t)$, respectively. Then, the sample covariance matrix is given by $\hat{\boldsymbol{R}} = \frac{1}{N}\boldsymbol{X}\boldsymbol{X}^{\mathrm{H}}$ such that assumptions A.1 and A.2 are only satisfied for $N \to \infty$. In the finite (small) sample case, however, $\hat{\boldsymbol{R}}$ is a poor estimate of $\boldsymbol{R}$ as assumptions A.1 and A.2 are not valid for $\hat{\boldsymbol{R}}$. In particular, expanding the sample covariance matrix, yields

$$\begin{aligned}\hat{\boldsymbol{R}} &= \frac{1}{N}(\boldsymbol{A}\boldsymbol{S} + \boldsymbol{N})(\boldsymbol{A}\boldsymbol{S} + \boldsymbol{N})^{\mathrm{H}} \\ &= \boldsymbol{A}\hat{\boldsymbol{R}}_{\mathrm{ss}}\boldsymbol{A}^{\mathrm{H}} + \boldsymbol{A}\hat{\boldsymbol{R}}_{\mathrm{sn}} + \hat{\boldsymbol{R}}_{\mathrm{ns}}\boldsymbol{A}^{\mathrm{H}} + \hat{\boldsymbol{R}}_{\mathrm{nn}} \\ &= \boldsymbol{A}\boldsymbol{R}_{\mathrm{ss}}\boldsymbol{A}^{\mathrm{H}} + \boldsymbol{A}(\hat{\boldsymbol{R}}_{\mathrm{ss}} - \boldsymbol{R}_{\mathrm{ss}})\boldsymbol{A}^{\mathrm{H}} \\ &\quad + \boldsymbol{A}\hat{\boldsymbol{R}}_{\mathrm{sn}} + \hat{\boldsymbol{R}}_{\mathrm{ns}}\boldsymbol{A}^{\mathrm{H}} + \boldsymbol{R}_{\mathrm{nn}} + (\hat{\boldsymbol{R}}_{\mathrm{nn}} - \boldsymbol{R}_{\mathrm{nn}}),\end{aligned} \tag{7}$$

where $\hat{\boldsymbol{R}}_{\mathrm{ss}} = \frac{1}{N}\boldsymbol{S}\boldsymbol{S}^{\mathrm{H}}$ and $\hat{\boldsymbol{R}}_{\mathrm{nn}} = \frac{1}{N}\boldsymbol{N}\boldsymbol{N}^{\mathrm{H}}$ are the sample estimates of $\boldsymbol{R}_{\mathrm{ss}}$ and $\boldsymbol{R}_{\mathrm{nn}}$, and $\hat{\boldsymbol{R}}_{\mathrm{sn}} = \frac{1}{N}\boldsymbol{S}\boldsymbol{N}^{\mathrm{H}}$ and $\hat{\boldsymbol{R}}_{\mathrm{ns}} = \frac{1}{N}\boldsymbol{N}\boldsymbol{S}^{\mathrm{H}}$ are the sample estimates of $\boldsymbol{R}_{\mathrm{sn}}$ and $\boldsymbol{R}_{\mathrm{ns}}$. Recall that $\lim_{N\to\infty}\hat{\boldsymbol{R}} = \boldsymbol{R}$. Comparing (7) to (4), three finite sample effects can be observed: the residual sample signal correlation $\hat{\boldsymbol{R}}_{\mathrm{ss}}$, which is non-diagonal, the residual sample noise correlation in the non-diagonal matrix $\hat{\boldsymbol{R}}_{\mathrm{nn}}$, and the non-zero sample cross-correlation matrices $\hat{\boldsymbol{R}}_{\mathrm{sn}}$ and $\hat{\boldsymbol{R}}_{\mathrm{ns}}$.

Define $\boldsymbol{N}_{\mathrm{n}} = \boldsymbol{A}\hat{\boldsymbol{R}}_{\mathrm{sn}} + \hat{\boldsymbol{R}}_{\mathrm{ns}}\boldsymbol{A}^{\mathrm{H}} + (\hat{\boldsymbol{R}}_{\mathrm{nn}} - \boldsymbol{R}_{\mathrm{nn}})$. Then, upon vectorizing (7), we obtain

$$\hat{\boldsymbol{z}} = \boldsymbol{A}_{\mathrm{v}}\boldsymbol{p} + \boldsymbol{A}_{\mathrm{r}}\boldsymbol{q} + \sigma_{\mathrm{n}}^2\boldsymbol{\Gamma}\boldsymbol{e} + \boldsymbol{n}_{\mathrm{n}}, \tag{8}$$

where $\boldsymbol{A}_{\mathrm{r}} = \boldsymbol{\Gamma}(\boldsymbol{A}^* \otimes \boldsymbol{A}) \in \mathbb{C}^{M^{\mathrm{sub}}\times d^2}$ and $\boldsymbol{q}$ contains the empirical source correlation $\hat{P}_{ij}$ for $i \neq j$ and $\hat{P}_i - P_i$ for $i = j$. Note that the second term represents the vectorized residual sample signal correlation while the last term $\boldsymbol{n}_{\mathrm{n}} = \boldsymbol{\Gamma}\,\mathrm{vec}\{\boldsymbol{N}_{\mathrm{n}}\}$ represents the vectorized residual sample noise and the signal-noise sample correlation.

III. Review of ESPRIT-type algorithms for Co-Arrays

Since $\boldsymbol{A}_{\mathrm{v}}$ in (8) represents a ULA, it satisfies the shift invariance property such that ESPRIT-type algorithms can be applied to estimate the spatial frequencies. The shift invariance equation is given by $\boldsymbol{J}_1\boldsymbol{A}_{\mathrm{v}}\boldsymbol{\Phi} = \boldsymbol{J}_2\boldsymbol{A}_{\mathrm{v}}$, where $\boldsymbol{J}_1$ and $\boldsymbol{J}_2 \in \mathbb{R}^{(M^{\mathrm{sub}}-1)\times M^{\mathrm{sub}}}$ are the selection matrices for the first and the second subarray with maximum overlap, and $\boldsymbol{\Phi} = \mathrm{diag}\{\mathrm{e}^{\mathrm{j}\mu_i}\}_{i=1}^{d} \in \mathbb{C}^{d\times d}$ contains the spatial frequencies of interest. Recall that (6) is a single snapshot model. Thus, spatial smoothing is required as preprocessing to restore the rank d before applying ESPRIT-type algorithms. To this end, the virtual ULA with M_{v} sensors is divided into L maximally overlapping subarrays, each containing $M_{\mathrm{v}}^{\mathrm{sub}} = M_{\mathrm{v}} - L + 1$ sensor elements. Let the selection matrix that corresponds to the ℓ-th subarray, $1 \leq \ell \leq L$, be defined as

$$\boldsymbol{J}_{\ell}^{(M_{\mathrm{v}})} = [\boldsymbol{0}_{M_{\mathrm{v}}^{\mathrm{sub}}\times(\ell-1)} \quad \boldsymbol{I}_{M_{\mathrm{v}}^{\mathrm{sub}}} \quad \boldsymbol{0}_{M_{\mathrm{v}}^{\mathrm{sub}}\times(L-\ell)}] \in \mathbb{R}^{M_{\mathrm{v}}^{\mathrm{sub}}\times M_{\mathrm{v}}}. \tag{9}$$

The spatially smoothed data matrix $\hat{\boldsymbol{Z}}_{\mathrm{SS}}$, which is subsequently processed instead of $\boldsymbol{z}$, is given by

$$\begin{aligned}\hat{\boldsymbol{Z}}_{\mathrm{SS}} &= \left[\boldsymbol{J}_1^{(M_{\mathrm{v}})}\hat{\boldsymbol{z}} \quad \boldsymbol{J}_2^{(M_{\mathrm{v}})}\hat{\boldsymbol{z}} \quad \cdots \quad \boldsymbol{J}_L^{(M_{\mathrm{v}})}\hat{\boldsymbol{z}}\right] \in \mathbb{C}^{M_{\mathrm{v}}^{\mathrm{sub}}\times L} \\ &= \left[\boldsymbol{J}_1^{(M_{\mathrm{v}})}\boldsymbol{A}_{\mathrm{v}}\boldsymbol{p} \ \cdots \ \boldsymbol{J}_L^{(M_{\mathrm{v}})}\boldsymbol{A}_{\mathrm{v}}\boldsymbol{p}\right] + \left[\boldsymbol{J}_1^{(M_{\mathrm{v}})}\boldsymbol{A}_{\mathrm{r}}\boldsymbol{q} \ \cdots \ \boldsymbol{J}_L^{(M_{\mathrm{v}})}\boldsymbol{A}_{\mathrm{r}}\boldsymbol{q}\right] \\ &\quad + \sigma_{\mathrm{n}}^2\left[\boldsymbol{J}_1^{(M_{\mathrm{v}})}\boldsymbol{\Gamma}\boldsymbol{e} \ \cdots \ \boldsymbol{J}_L^{(M_{\mathrm{v}})}\boldsymbol{\Gamma}\boldsymbol{e}\right] + \left[\boldsymbol{J}_1^{(M_{\mathrm{v}})}\boldsymbol{n}_{\mathrm{n}} \ \cdots \ \boldsymbol{J}_L^{(M_{\mathrm{v}})}\boldsymbol{n}_{\mathrm{n}}\right] \\ &= \boldsymbol{Z}_{0\mathrm{SS}} + \boldsymbol{Z}_{\mathrm{rSS}} + \boldsymbol{\Xi}_{0\mathrm{SS}} + \boldsymbol{\Xi}_{\mathrm{nSS}} \\ &= \boldsymbol{Z}_{0\mathrm{SS}} + \boldsymbol{Z}_{\mathrm{rSS}} + \boldsymbol{\Xi}_{\mathrm{SS}},\end{aligned} \tag{10}$$

where $\boldsymbol{Z}_{0\mathrm{SS}}$ is the noise-free spatially smoothed data matrix (infinite sample size), $\boldsymbol{Z}_{\mathrm{rSS}}$ is the residual sample signal correlation, and $\boldsymbol{\Xi}_{\mathrm{SS}} = \boldsymbol{\Xi}_{0\mathrm{SS}} + \boldsymbol{\Xi}_{\mathrm{nSS}}$ contains the sample noise contribution. Note that we require $\min\{M_{\mathrm{v}} - L, L\} \geq d$ to estimate the d spatial frequencies. Furthermore, $\boldsymbol{Z}_{0\mathrm{SS}}$ can be equivalently expressed as

$$\boldsymbol{Z}_{0\mathrm{SS}} = \boldsymbol{J}_1^{(M_{\mathrm{v}})} \boldsymbol{A}_{\mathrm{v}} \left[\boldsymbol{p}, \boldsymbol{\Phi}\boldsymbol{p}, \cdots, \boldsymbol{\Phi}^{L-1}\boldsymbol{p}\right] = \boldsymbol{A}_{\mathrm{v}_1} \bar{\boldsymbol{\Phi}} \left(\boldsymbol{I}_L \otimes \boldsymbol{p}\right), \quad (11)$$

where $\boldsymbol{A}_{\mathrm{v}_1} = \boldsymbol{J}_1^{(M_{\mathrm{v}})} \boldsymbol{A}_{\mathrm{v}}$ and $\bar{\boldsymbol{\Phi}} = [\boldsymbol{I}_d, \boldsymbol{\Phi}, \ldots, \boldsymbol{\Phi}^{L-1}]$. It is apparent that $\boldsymbol{A}_{\mathrm{v}_1}$ still satisfies the shift invariance equation, i.e.,

$$\boldsymbol{J}_{\mathrm{SS}_1} \boldsymbol{A}_{\mathrm{v}_1} \boldsymbol{\Phi} = \boldsymbol{J}_{\mathrm{SS}_2} \boldsymbol{A}_{\mathrm{v}_1}, \quad (12)$$

where $\boldsymbol{J}_{\mathrm{SS}_1}$ and $\boldsymbol{J}_{\mathrm{SS}_2} \in \mathbb{R}^{(M_{\mathrm{v}}^{\mathrm{sub}}-1) \times M_{\mathrm{v}}^{\mathrm{sub}}}$ are the selection matrices, which select $M_{\mathrm{v}}^{\mathrm{sub}} - 1$ out of $M_{\mathrm{v}}^{\mathrm{sub}}$ sensors for the first and second subarray, respectively. As $\boldsymbol{A}_{\mathrm{v}_1}$ is unknown in practice, an estimate $\hat{\boldsymbol{U}}_{\mathrm{SS_s}}$ of the corresponding signal subspace $\boldsymbol{U}_{\mathrm{SS_s}}$ is obtained by computing the d dominant left singular vectors of $\boldsymbol{Z}_{\mathrm{SS}}$. Using the fact that $\boldsymbol{A}_{\mathrm{v}_1}$ and $\hat{\boldsymbol{U}}_{\mathrm{SS_s}}$ span approximately the same column space, a non-singular matrix $\boldsymbol{T} \in \mathbb{C}^{d \times d}$ can be found such that $\boldsymbol{A}_{\mathrm{v}_1} \approx \hat{\boldsymbol{U}}_{\mathrm{SS_s}} \boldsymbol{T}$. With this relation, the shift invariance equation can be expressed in terms of $\hat{\boldsymbol{U}}_{\mathrm{SS_s}}$, i.e., $\boldsymbol{J}_{\mathrm{SS}_1} \hat{\boldsymbol{U}}_{\mathrm{SS_s}} \boldsymbol{\Upsilon} \approx \boldsymbol{J}_{\mathrm{SS}_2} \hat{\boldsymbol{U}}_{\mathrm{SS_s}}$ with $\boldsymbol{\Upsilon} \approx \boldsymbol{T}\boldsymbol{\Phi}\boldsymbol{T}^{-1}$. Often, the unknown matrix $\boldsymbol{\Upsilon}$ is estimated using least squares (LS), i.e., $\hat{\boldsymbol{\Upsilon}} = (\boldsymbol{J}_{\mathrm{SS}_1} \hat{\boldsymbol{U}}_{\mathrm{SS_s}})^{+} \boldsymbol{J}_{\mathrm{SS}_2} \hat{\boldsymbol{U}}_{\mathrm{SS_s}} \in \mathbb{C}^{d \times d}$, where $^{+}$ stands for the Moore-Penrose pseudo inverse. Then, the spatial frequency estimates are extracted from the eigenvalues $\hat{\lambda}_i$ of the solution $\hat{\boldsymbol{\Upsilon}}$ via $\hat{\mu}_i = \arg\{\hat{\lambda}_i\}$. Alternatively, Unitary ESPRIT [3] can be applied to estimate the spatial frequencies.

IV. Performance of Standard ESPRIT for Co-Arrays

For the perturbation analysis of the estimation error, we adopt the analytical framework proposed in [11] and [12]. Therein, an explicit first-order error expansion is derived assuming that the additive perturbation is deterministic (potentially non-Gaussian) and small compared to the signal. These assumptions are not violated by the co-array preprocessing such that [11] and [12] are still applicable. Moreover, the performance analysis framework allows to investigate the finite sample effects.

Starting with the derivation of the signal subspace estimation error based on (10), we first write the SVD of the noise-free data matrix $\boldsymbol{Z}_{0\mathrm{SS}}$ as

$$\boldsymbol{Z}_{0\mathrm{SS}} = \begin{bmatrix}\boldsymbol{U}_{\mathrm{SS_s}} & \boldsymbol{U}_{\mathrm{SS_n}}\end{bmatrix} \begin{bmatrix}\boldsymbol{\Sigma}_{\mathrm{SS_s}} & \boldsymbol{0} \\ \boldsymbol{0} & \boldsymbol{0}\end{bmatrix} \begin{bmatrix}\boldsymbol{V}_{\mathrm{SS_s}} & \boldsymbol{V}_{\mathrm{SS_n}}\end{bmatrix}^{\mathrm{H}}, \quad (13)$$

where $\boldsymbol{U}_{\mathrm{SS_s}} \in \mathbb{C}^{M_{\mathrm{v}}^{\mathrm{sub}} \times d}$, $\boldsymbol{U}_{\mathrm{SS_n}} \in \mathbb{C}^{M_{\mathrm{v}}^{\mathrm{sub}} \times (L-d)}$, and $\boldsymbol{V}_{\mathrm{SS_s}} \in \mathbb{C}^{L \times d}$ span the signal subspace, the noise subspace, and the row space, respectively, and $\boldsymbol{\Sigma}_{\mathrm{SS_s}} \in \mathbb{R}^{d \times d}$ contains the non-zero singular values on its diagonal.

Next, we express the signal subspace estimate $\hat{\boldsymbol{U}}_{\mathrm{SS_s}}$ in terms of $\boldsymbol{U}_{\mathrm{SS_s}}$ as $\hat{\boldsymbol{U}}_{\mathrm{SS_s}} = \boldsymbol{U}_{\mathrm{SS_s}} + \Delta\boldsymbol{U}_{\mathrm{SS_s}}$, where $\Delta\boldsymbol{U}_{\mathrm{SS_s}}$ denotes the subspace estimation error. Then, the first-order approximation of the subspace error is given by [11], [12]

$$\Delta\boldsymbol{U}_{\mathrm{SS_s}} \approx \boldsymbol{U}_{\mathrm{SS_n}} \boldsymbol{U}_{\mathrm{SS_n}}^{\mathrm{H}} \left(\boldsymbol{Z}_{\mathrm{rSS}} + \boldsymbol{\Xi}_{\mathrm{SS}}\right) \boldsymbol{V}_{\mathrm{SS_s}} \boldsymbol{\Sigma}_{\mathrm{SS_s}}^{-1}. \quad (14)$$

Following [12], the estimation error of the i-th spatial frequency using the LS to solve the shift invariance equation is obtained as

$$\Delta\mu_i \approx \mathrm{Im}\left\{\boldsymbol{p}_i^{\mathrm{T}} \left(\boldsymbol{J}_{\mathrm{SS}1} \boldsymbol{U}_{\mathrm{SS_s}}\right)^{+} \left[\boldsymbol{J}_{\mathrm{SS}2}/\lambda_i - \boldsymbol{J}_{\mathrm{SS}1}\right] \Delta\boldsymbol{U}_{\mathrm{SS_s}} \boldsymbol{q}_i\right\}, \quad (15)$$

where $\lambda_i = \mathrm{e}^{\mathrm{j}\mu_i}$ is the i-th eigenvalue of $\boldsymbol{\Upsilon}$, and the vectors $\boldsymbol{q}_i$ and $\boldsymbol{p}_i$ represent the respective i-th columns of the matrices $\boldsymbol{Q}$ and $\boldsymbol{P} = \boldsymbol{Q}^{-1}$, which result from the eigendecomposition $\boldsymbol{\Upsilon} = \boldsymbol{Q}\boldsymbol{\Lambda}\boldsymbol{Q}^{-1}$.

Finally, the MSE of the i-th spatial frequency using co-array-based Standard ESPRIT is given by $\mathbb{E}\left\{(\Delta\mu_i)^2\right\}$.

V. Performance of Unitary ESPRIT for Co-Arrays

In this section, we derive the analytical performance expressions of Unitary ESPRIT for co-arrays. The additional features of Unitary ESPRIT compared to Standard ESPRIT are the incorporation of forward-backward averaging (FBA) and the real-valued transformation to reduce the computational complexity [3].

It was shown in [14], [15] that only FBA needs to be considered for the first-order performance analysis of Unitary-ESPRIT-type algorithms. FBA is performed by replacing the spatially smoothed data matrix $\boldsymbol{Z}_{\mathrm{SS}} \in \mathbb{C}^{M_{\mathrm{v}}^{\mathrm{sub}} \times L}$ by the column-augmented data matrix $\tilde{\boldsymbol{Z}}_{\mathrm{SS}} \in \mathbb{C}^{M_{\mathrm{v}}^{\mathrm{sub}} \times 2L}$ defined by

$$\tilde{\boldsymbol{Z}}_{\mathrm{SS}} = \begin{bmatrix}\boldsymbol{Z}_{\mathrm{SS}} & \boldsymbol{\Pi}_{M_{\mathrm{v}}^{\mathrm{sub}}} \boldsymbol{Z}_{\mathrm{SS}}^{*} \boldsymbol{\Pi}_L\end{bmatrix} = \tilde{\boldsymbol{Z}}_{0\mathrm{SS}} + \tilde{\boldsymbol{Z}}_{\mathrm{rSS}} + \tilde{\boldsymbol{\Xi}}_{\mathrm{SS}}, \quad (16)$$

where $\tilde{\boldsymbol{Z}}_{0\mathrm{SS}}$ is the noise-free FBA-processed data matrix. The transformation (16) does not alter the assumptions made in the previous subsection. Hence, the same performance analysis framework is still applicable to (16). We replace the noise-free subspaces of $\boldsymbol{Z}_{0\mathrm{SS}}$ in (15) by the corresponding subspaces of $\tilde{\boldsymbol{Z}}_{0\mathrm{SS}}$, and $\boldsymbol{p}_i$ and $\boldsymbol{q}_i$ by $\tilde{\boldsymbol{p}}_i$ and $\tilde{\boldsymbol{q}}_i$, respectively, to obtain the first-order expression for the i-th spatial frequency as

$$\Delta\tilde{\mu}_i \approx \mathrm{Im}\left\{\tilde{\boldsymbol{p}}_i^{\mathrm{T}} \left(\boldsymbol{J}_{\mathrm{SS}1} \tilde{\boldsymbol{U}}_{\mathrm{SS_s}}\right)^{+} \left[\boldsymbol{J}_{\mathrm{SS}2}/\lambda_i - \boldsymbol{J}_{\mathrm{SS}1}\right] \Delta\tilde{\boldsymbol{U}}_{\mathrm{SS_s}} \tilde{\boldsymbol{q}}_i\right\}, \quad (17)$$

where the signal subspace error $\Delta\tilde{\boldsymbol{U}}_{\mathrm{SS_s}} \in \mathbb{C}^{M_{\mathrm{v}}^{\mathrm{sub}} \times d}$ is given by

$$\Delta\tilde{\boldsymbol{U}}_{\mathrm{SS_s}} \approx \tilde{\boldsymbol{U}}_{\mathrm{SS_n}} \tilde{\boldsymbol{U}}_{\mathrm{SS_n}}^{\mathrm{H}} \left(\tilde{\boldsymbol{Z}}_{\mathrm{rSS}} + \tilde{\boldsymbol{\Xi}}_{\mathrm{SS}}\right) \tilde{\boldsymbol{V}}_{\mathrm{SS_s}} \tilde{\boldsymbol{\Sigma}}_{\mathrm{SS_s}}^{-1}. \quad (18)$$

Then, the MSE of the i-th spatial frequency of co-array-based Unitary ESPRIT is given by $\mathbb{E}\left\{(\Delta\tilde{\mu}_i)^2\right\}$.

VI. Simulation Results

In this section, we show numerical results to evaluate the estimation accuracy of the proposed co-array-based Standard ESPRIT (CA SE) and co-array-based Unitary ESPRIT (CA UE) algorithms along with their performance analysis. In particular, we compare the empirical (emp) estimation error using Monte-Carlo trials to the derived analytical (ana) MSE expressions. Both algorithms are benchmarked by the corresponding stochastic Cramér-Rao bound (Sto CA CRB) [13]. We consider a nested array with $M = 6$ sensors and the sparse sensor configuration $\boldsymbol{k} = [1, 2, 3, 4, 8, 12]\frac{\lambda}{2}$. We have $M_{\mathrm{v}} = 23$ and choose $L = 12$ for spatial smoothing. We assume that the sources have unit power and that the transmit symbols are drawn from a complex Gaussian distribution. The noise is zero-mean circularly symmetric complex Gaussian and 5000 trials are used to generate the plots.

To study the effect of the residual sample signal correlation and the residual sample noise and signal-noise correlation on the estimation accuracy of the algorithms, we compare the case of the residual sample signal correlation (rssc) (only $\boldsymbol{Z}_{\mathrm{rSS}}$ enters (14) and there is no noise) to the case of all sample effects (sample) ($\boldsymbol{Z}_{\mathrm{rSS}}$ and $\boldsymbol{\Xi}_{\mathrm{SS}}$ enter (14)) in a semi-algebraic fashion. In the simulations, we additionally investigate the case of fewer sources than sensors ($d < M$) followed by the case of more sources than sensors ($d > M$). As a reference for the former, we also include the conventional Standard ESPRIT and Unitary ESPRIT algorithms along with the stochastic CRB based on a ULA with $M = 6$ sensors. Note that the ULA shares the same number of sensors with the sparse linear array, but has a smaller aperture. Moreover, least squares (LS) is used to solve the shift invariance equation for the ESPRIT algorithms.

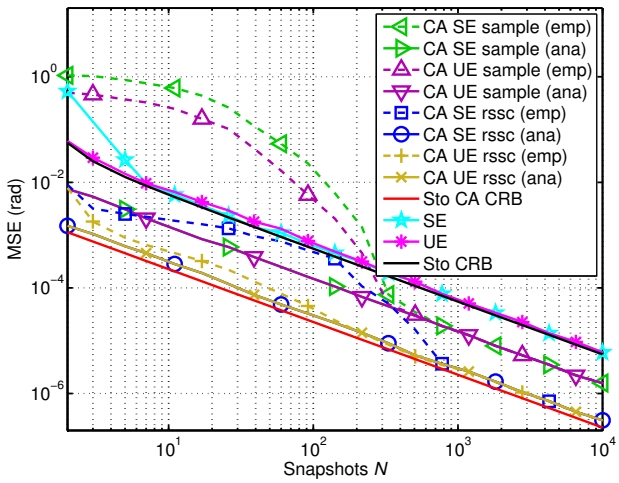

Fig. 1. MSE versus N with SNR = 20 dB, $d = 2$ sources at $\mu_1 = 0$ and $\mu_2 = 0.1$.

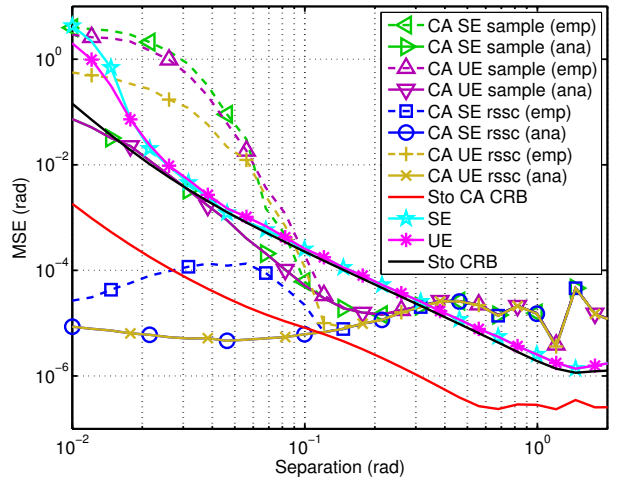

Fig. 2. MSE versus source separation with SNR = 20 dB, $N = 500$, $d = 2$ sources.

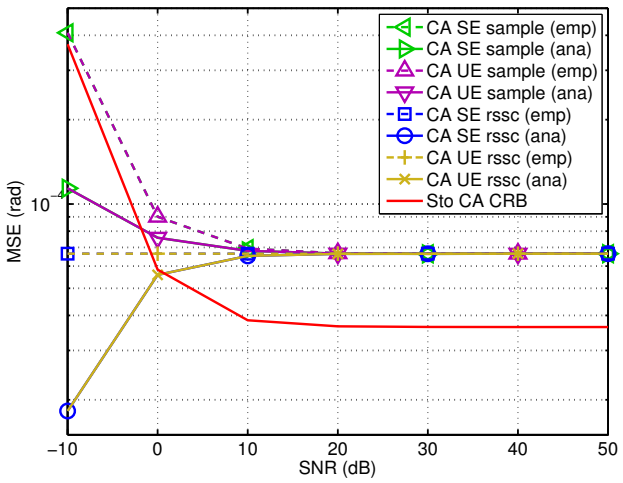

Fig. 3. MSE versus SNR with $N = 10^4$, $d = 11$ sources uniformly spaced between $-10/11\pi$ and $10/11\pi$.

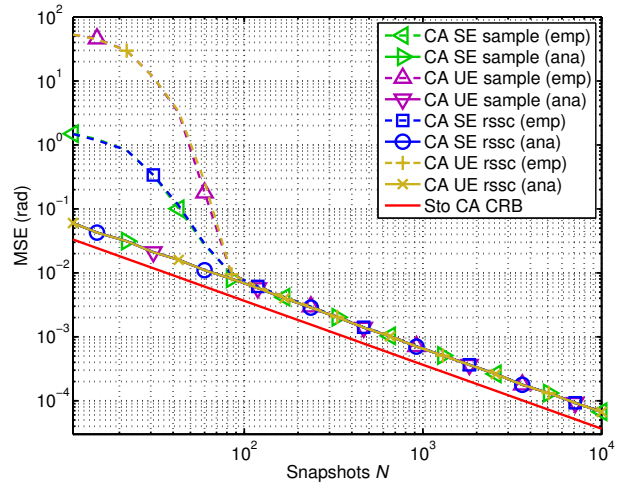

Fig. 4. MSE versus N with SNR = 20 dB, $d = 11$ sources uniformly spaced between $-10/11\pi$ and $10/11\pi$.

A. Fewer Sources Than Sensors

Fig. 1 illustrates the total mean square error (MSE) versus the number of snapshots N. We have $d = 2$ sources located at $\mu_1 = 0$ and $\mu_2 = 0.1$ with SNR = 20 dB. It is apparent that around $N = 400$ is required for the empirical curves to match the analytical ones. Moreover, the effect of the residual sample noise and signal-noise correlation is more severe than that of the residual sample signal correlation. Both CA ESPRIT methods outperform the conventional ESPRIT methods for the ULA for $N > 400$. In Fig. 2, we depict the MSE versus the separation of $d = 2$ sources. To this end, we fix $\mu_1 = -\pi/2$ and increase the distance of μ_2. We set $N = 500$ and SNR = 20 dB. It can be observed that the empirical and analytical curves match from $\Delta\mu = |\mu_2 - \mu_1| = 0.2$ rad. Surprisingly, in the case of fewer sources than sensors, the CA-based ESPRIT methods outperform the conventional methods only for a small separation range. This effect remains to be investigated.

B. More Sources Than Sensors

Fig. 3 shows the MSE versus the SNR for $d = 11$ uniformly spaced sources between $-10/11\pi$ and $10/11\pi$ and $N = 10^4$. Note that the conventional methods cannot resolve more sources than sensors. First, we notice the error floor as the SNR increases. This effect has already been observed in [13]. From the analytical curve for the residual signal correlation, it is apparent that the error floor is only due to this effect. The empirical and analytical curves match at SNR = 20 dB. In Fig. 4, we provide the MSE versus the sample size N. We keep $d = 11$ and the signal positions and fix the SNR to 20 dB. From $N = 100$, the empirical and analytical curves match. Moreover, the MSE of the CA-based ESPRIT algorithms tends to zero as the residual sample signal correlation decreases with increasing N. The algorithms perform close to the CA CRB. In summary, the simulations also verify that the presented analytical performance evaluation is asymptotic in the high effective SNR, i.e., the results become exact for either high SNRs or a large sample size.

VII. Conclusion

In this paper, we have reviewed the Standard ESPRIT and Unitary ESPRIT algorithms for the co-array processing of sparse linear arrays. Additionally, we have presented a first-order performance analysis of both algorithms, which is asymptotic in the effective SNR and therefore also valid for a small sample size. Using these analytical expressions, we have studied the effects of a small sample size that results in a residual sample signal and sample noise correlation on the estimation error of the proposed co-array-based ESPRIT-type algorithms. The derived expressions are verified by simulations.

REFERENCES

[1] H. Krim and M. Viberg, "Two decades of array signal processing research: the parametric approach," *IEEE Signal Processing Magazine*, vol. 13, no. 4, pp. 67-94, July 1996.

[2] R. H. Roy and T. Kailath, "ESPRIT-estimation of signal parameters via rotational invariance techniques," *IEEE Transactions on Acoustics, Speech, and Signal Processing*, vol. 37, no. 7, pp. 984-995, July 1989.

[3] M. Haardt and J. A. Nossek, "Unitary ESPRIT: How to obtain increased estimation accuracy with a reduced computational burden," *IEEE Trans. on Signal Processing*, vol. 43, no. 5, pp. 1232-1242, May 1995.

[4] A. Moffet, "Minimum-redundancy linear arrays," *IEEE Transactions on Antennas and Propagation*, vol. 16, no. 2, pp. 172-175, Mar. 1968.

[5] P. Pal and P. Vaidyanathan, "Nested arrays: A novel approach to array processing with enhanced degrees of freedom," *IEEE Transactions on Signal Processing*, vol. 58, no. 8, pp. 4167-4181, Aug. 2010.

[6] P. P. Vaidyanathan and P. Pal, "Sparse sensing with co-prime samplers and arrays," *IEEE Transactions on Signal Processing*, vol. 59, no. 2, pp. 573-586, Feb. 2011.

[7] A. Liu, Q. Yang, X. Zhang, and W. Deng, "Direction-of-Arrival Estimation for Coprime Array Using Compressive Sensing Based Array Interpolation," *Hindawi International Journal of Antennas and Propagation*, vol. 2017, Feb. 2017.

[8] T.-J. Shan, M. Wax, and T. Kailath, "On spatial smoothing for direction-of-arrival estimation of coherent signals," *IEEE Transactions on Acoustics, Speech, and Signal Processing*, vol. 33, no. 4, pp. 806-811, Aug. 1985.

[9] P. Stoica and A. Nehorai, "MUSIC, maximum likelihood, and Cramer-Rao bound," *IEEE Transactions on Acoustics, Speech and Signal Processing*, vol. 37, no. 5, pp. 720-741, May 1989.

[10] B. D. Rao and K. V. S. Hari, "Performance analysis of ESPRIT and TAM in determining the direction of arrival of plane waves in noise," *IEEE Transactions on Acoustics, Speech, and Signal Processing*, vol. 37, no. 12, pp. 1990-1995, Dec. 1989.

[11] F. Li, H. Liu, and R. J. Vaccaro, "Performance analysis for DOA estimation algorithms: Unification, simplifications, and observations," *IEEE Transactions on Aerospace and Electronic Systems*, vol. 29, no. 4, pp. 1170-1184, Oct. 1993.

[12] J. Steinwandt, F. Roemer, M. Haardt, and G. Del Galdo, "Performance analysis of multi-dimensional ESPRIT-type algorithms for arbitrary and strictly non-circular sources with spatial smoothing," *IEEE Transactions on Signal Processing*, vol. 65, no. 9, pp. 2262-2276, May 2017.

[13] M. Wang and A. Nehorai, "Coarrays, MUSIC, and the Cramér-Rao bound," *IEEE Transactions on Signal Processing*, vol. 65, no. 4, pp. 933-946, Feb. 2017.

[14] F. Roemer, M. Haardt, and G. Del Galdo, "Analytical performance assessment of multi-dimensional matrix- and tensor-based ESPRIT-type algorithms," *IEEE Transactions on Signal Processing*, vol. 62, pp. 2611-2625, May 2014.

[15] J. Steinwandt, F. Roemer, M. Haardt, and G. Del Galdo, "R-dimensional ESPRIT-type algorithms for strictly second-order non-circular sources and their performance analysis," *IEEE Transactions on Signal Processing*, vol. 62, no. 18, pp. 4824-4838, Sep. 2014.